JUSTC

Article

http://justc.ustc.edu.cn

Received: July 31, 2025; Accepted: October 15, 2025

The motion of the magnetic flux tube in the Earth's low-latitude boundary layer under northward IMF conditions

Xinling Ma, and Chuxin Chen ✉

School of Earth and Space Sciences, University of Science and Technology of China, Hefei 230026, China

✉Correspondence: Chuxin Chen, E-mail: chuxin@ustc.edu.cn

Graphical abstract

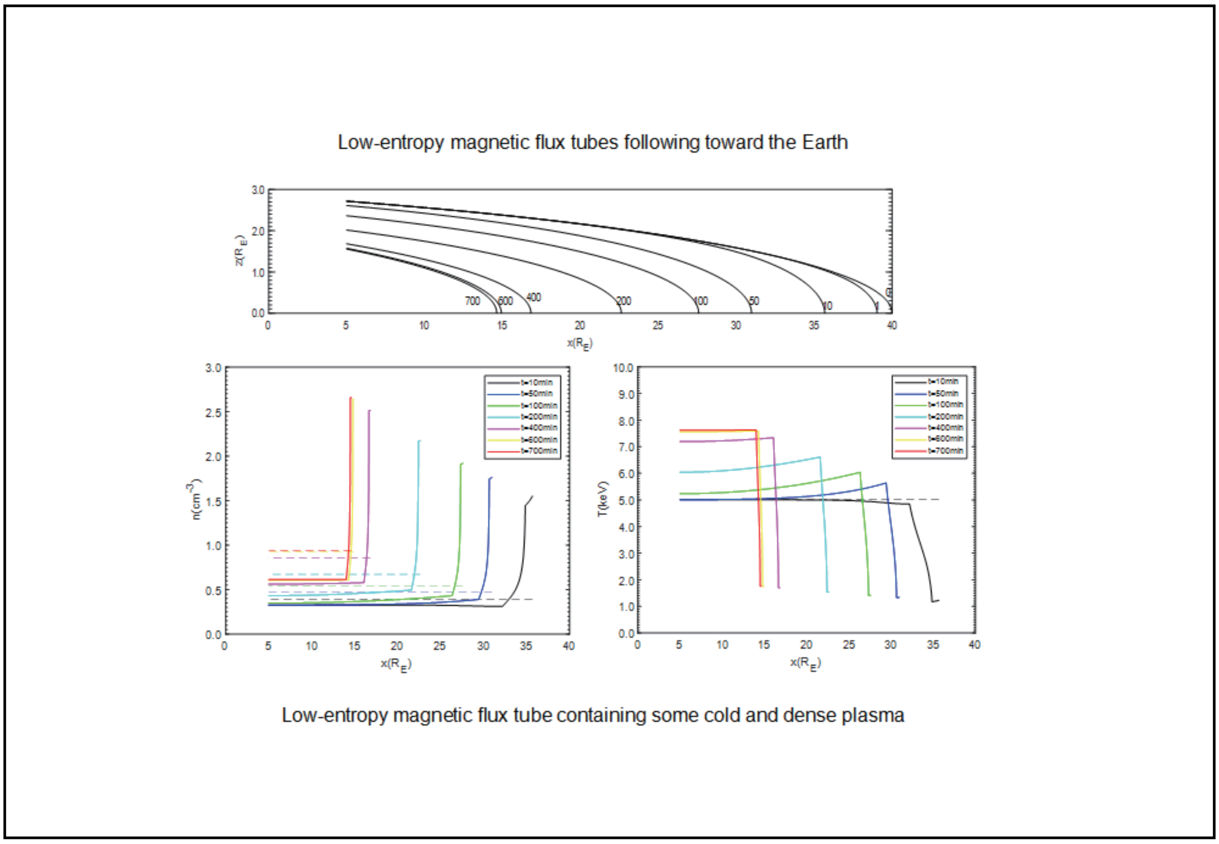

1D simulation results of the motion of magnetic flux tube.

Public summary

- A 1D MHD numerical method is adopted to efficiently capture the earthward movement of magnetic flux tubes at the magnetospheric flank under northward IMF condition.
- The sunward motion of these conjugate reconnection-generated flux tubes along the magnetospheric flanks is consistent with the typical four-cell convection pattern in the polar cap under northward IMF.
- The transfer of magnetosheath particles into the Earth's magnetosphere contributes to the formation of the typical cold and dense plasma sheet under northward IMF.

Citation: Ma X L, Chen C X. The motion of the magnetic flux tube in the Earth's low-latitude boundary layer under northward IMF conditions. *JUSTC*, **2025**, 55(0): . CSTR: 32290.14.JUSTC-2025-0077. DOI: 10.52396/JUSTC-2025-0077

JUSTC Article
http://justc.ustc.edu.cn
Received: July 31, 2025; Accepted: October 15, 2025

The motion of the magnetic flux tube in the Earth's low-latitude boundary layer under northward IMF conditions

Xinling Ma, and Chuxin Chen ✉

School of Earth and Space Sciences, University of Science and Technology of China, Hefei 230026, China

✉Correspondence: Chuxin Chen, E-mail: chuxin@ustc.edu.cn

Cite This: *JUSTC*, **2025**, 55(X): (8pp) Read Online

Abstract: How solar wind plasma enters the Earth's magnetosphere when the interplanetary magnetic field (IMF) is northward is an active research topic.To further demonstrate that the Kelvin–Helmholtz instability (KHI) is the main mechanism by which particles of the solar wind enter Earth's magnetosphere , we use numerical simulation methods to study the motion of magnetic flux tubes at the Earth's magnetospheric flanks. These magnetic flux tubes are obtained through conjugate reconnection in the nonlinear stage of the KHI. The part of the original magnetic flux tube of the magnetosphere near the equator was replaced by a part of the magnetic flux tube of the magnetosheath. The reconnected magnetic flux tube, which contains a large number of magnetosheath particles, forms a low-entropy magnetic flux tube.The simulation results indicate that the reconnected magnetic flux tube flows toward the Sun along the magnetospheric flanks. This is consistent with the sunward flow in the center of the polar cap under northward IMF conditions. Analysis of the internal parameters of the flowing magnetic flux tube reveals that the newborn magnetic flux tube contributes to the formation of a cold and dense plasma sheet.

Keywords: northward IMF; Kelvin–Helmholtz instability; conjugate reconnection; low-entropy magnetic flux tube

CLC number: P353 **Document code:** A

1 Introduction

The Earth's magnetosphere is an obstacle to solar wind. They are generally considered to be nonpenetrative to each other. However, shortly after the launch of satellites, it was discovered that the Earth's magnetosphere is filled with solar-originated plasma. How solar wind plasma enters the magnetosphere has long been an important research topic. When the interplanetary magnetic field (IMF) is southward, the plasma sheet in the Earth's magnetosphere is filled with tenuous and hot plasma. It is now generally accepted that magnetic reconnection is the main mechanism for solar wind plasma to enter the magnetosphere under this IMF condition[1]. The southward IMF reconnects with the northward magnetic field of the Earth's magnetosphere at the subsolar point on the dayside magnetopause, resulting in open magnetic field lines moving with magnetosheath particles toward the magnetotail. Another magnetic reconnection occurs at the magnetotail, converting open magnetic field lines into closed lines and thereby transporting many solar wind particles into the magnetosphere[2,3]. When the direction of the IMF turns away from southward, the situation becomes complicated, and both magnetic reconnection and viscous effects play roles[4,5]. Cold and dense plasma is observed in the plasma sheet when the IMF is northward. Scientists have proposed various transport mechanisms for solar wind plasma entering the magnetosphere under such IMF conditions. They include magnetic reconnection at high-latitude cusp regions at the nightside[6], Kelvin–Helmholtz instability (KHI) at the magnetospheric flanks[7], kinetic Alfvén waves (KAWs) in the magnetosheath[8], and direct impulsive penetration of inhomogeneous structures in the magnetosheath[9]. These mechanisms may coexist, but their relative importance remains highly controversial[10]. Thus, the transport mechanism of solar wind plasma into the magnetosphere under a northward IMF is an active research topic.

Both double-cusp reconnection at high latitudes and KHI at the magnetospheric flanks are considered effective for transporting solar wind plasma under the northward IMF. Through these two mechanisms, particles entering the magnetosphere may form a low-latitude boundary layer (LLBL) near the equator over time, which accumulates to form a cold and dense plasma sheet (CDPS) in the magnetotail[11]. In 2015, Kavosi and Raeder[12] further confirmed the significance of the KHI. With statistical data, they showed that KHI occurs 19% of the time regardless of solar wind and IMF conditions, suggesting a more important role of KHI than previously thought. Notably, on the basis of observations that the ion-to-electron temperature ratio remains constant while the specific entropy increases by 2–3 orders of magnitude when crossing the magnetopause, Chen [13] concluded that magnetic reconnection during the nonlinear stage of KHI is the main process by which solar-originated plasma enters the magnetosphere under the northward IMF. This conjugate reconnection[14,15] occurs at low latitudes (with one reconnection site on the north side of the neutral sheet and the other site at its conjugate point on the south side of the neutral sheet). A part of the

CSTR: 32290.14.JUSTC-2025-0077
DOI: 10.52396/JUSTC-2025-0077
JUSTC, **2025**, 55(X):

magnetospheric flux tube near the equator is replaced by a part of the magnetosheath flux tube, resulting in a low-entropy flux tube[15–17]. In this study, we use numerical simulations to further explore the relative importance of entry mechanisms for KHI.

Numerical methods, including local resistive magnetohydrodynamic (MHD) simulations, global MHD simulations, and hybrid and kinetic simulations, have been widely applied to study the evolution of KHIs. Guo et al.[18] used global MHD simulations to show that KHI occurs at the low-latitude magnetopause under the northward IMF, presenting a global picture of the nonlinear evolution of KHI. Sorathia et al.[19] combined global MHD and test particle simulations to model solar wind ions entering the magnetosphere during northward IMF and compared the transport rates of KHIs.

In this work, to further evaluate the role of KHI in solar wind plasma entry into the magnetosphere, we employ a 1D MHD numerical method to study the motion of magnetic flux tubes in the LLBL during the northward IMF. These magnetic flux tubes are low-entropy magnetic flux tubes produced by replacing a part of the magnetospheric flux tube near the equator with a part of the magnetosheath flux tube during the nonlinear stage of KHI. The model is introduced in Section 2, the results are presented in Section 3, and the conclusions and discussion are presented in Section 4.

2 Model

We establish our model in a Cartesian coordinate system. The x-axis points from the Sun toward the Earth, the z-axis points from the geomagnetic south pole to the geomagnetic north pole, and the y-axis completes the right-handed orthogonal system, pointing from dusk to dawn. The new magnetic flux tubes generated by conjugate reconnection in the nonlinear stage of KHI under the northward IMF are treated as a 1D filament, and the background magnetosphere is treated as a 2D medium. Both our 1D filament and the background magnetic field lines are confined on the xz plane. The background medium exerts only a small viscous drag on the filament, which can slide between the background magnetic field lines. Pontius and Wolf[20] proposed that the scale of the magnetic filament near the neutral sheet on the Earth's equatorial plane is approximately 1 R_E on the basis of interchange instability. In our model, the scale of the magnetic filament on the equatorial plane is also set to 1 R_E. The 2D background we constructed in this study can be understood as a cross-section of the Earth's magnetosphere in the xz directions. Motion on this plane can be interpreted as the motion of magnetic flux tubes along the magnetospheric flanks (the filament cannot cross the background plane but only slides on it). Thus, the descriptions "motion toward the Earth" and "motion toward the Sun" in the text are equivalent, with "Earth" located on the left side of the 2D background.

2.1 Background model

When the background medium is in equilibrium, the momentum equation is

$$\nabla P = \boldsymbol{j} \times \boldsymbol{B}, \tag{1}$$

where P is the thermal pressure, $\boldsymbol{j}$ is the current density, and $\boldsymbol{B}$ is the magnetic field. From Eq. (1), we derive

$$\boldsymbol{B} \cdot \nabla P = 0. \tag{2}$$

The pressure P is constant along the magnetic field lines. Let

$$\boldsymbol{B} = \nabla \times \boldsymbol{A}, \tag{3}$$

where $\boldsymbol{A}$ is the magnetic vector potential. In the 2D model, $\boldsymbol{B} \cdot \nabla A = 0$, so A is also constant along the magnetic field lines. The magnetic vector potential satisfies the Grad–Shafranov condition[21], with the form

$$\nabla^2 A = -\mu_0 \frac{\mathrm{d}P}{\mathrm{d}A}. \tag{4}$$

According to the Fuchs–Voigt 2D force-balanced magnetic field model[22], A has the following form:

$$A_{\mathrm{med}}(x,z) = \frac{\pi A_0}{2\alpha\Delta} \sin\left[\alpha\left(|z| - \Delta\right)\right] \exp(-\alpha x), \quad |z| > \Delta; \tag{5a}$$

$$A_{\mathrm{med}}(x,z) = -A_0 \cos\left[\frac{\pi z}{2\Delta}\right] \exp(-\alpha x), \quad |z| \le \Delta, \tag{5b}$$

where $A_0 = 150\ \mathrm{nT}/R_E$, $\alpha = 0.0208 R_E^{-1}$, and Δ is set to 4 R_E, which is half of the plasma sheet thickness, and the background medium is denoted by the subscript "med". The thermal pressure P can be obtained by integrating Eq. (4):

$$P = 0, \quad |z| > \Delta; \tag{6a}$$

$$P(A) = \frac{A^2}{2\mu_0}\left[\left(\frac{\pi}{2\Delta}\right)^2 - \alpha^2\right], \quad |z| \le \Delta; \tag{6b}$$

Thus, the background medium model is established, where $|z| \le \Delta$ corresponds to the plasma sheet and $|z| > \Delta$ corresponds to the magnetomantle.

2.2 Filament motion equation

The shape of the filament in the Lagrangian method is denoted as $\boldsymbol{x}(m,t)$, and the corresponding velocity can be obtained

$$\boldsymbol{u}(m,t) = \frac{\partial \boldsymbol{x}(m,t)}{\partial t}, \tag{7}$$

where m is the mass of the filament between the equatorial plane and the point we discuss. The magnetic flux of the filament is conserved during motion, and the volume along the filament is

$$\mathrm{d}V = \frac{\Phi \mathrm{d}s}{B}, \tag{8}$$

where Φ is the magnetic flux of the filament, B is the magnetic field strength in the filament, and $\mathrm{d}s$ is the length element along the filament. The mass of the filament is

$$\mathrm{d}m = \frac{\rho \Phi \mathrm{d}s}{B}, \tag{9}$$

where ρ is the mass density. According to the frozen flux theorem in ideal MHD, the direction of the magnetic field remains along the filament during motion.

$$\boldsymbol{B} = \Phi\rho \frac{\partial \boldsymbol{x}(m,t)}{\partial m}. \tag{10}$$

CSTR: 32290.14.JUSTC-2025-0077
DOI: 10.52396/JUSTC-2025-0077
JUSTC, **2025**, 55(X):

The ideal gas law is

$$P = \frac{\rho k T}{\overline{m}}, \tag{11}$$

where k is the Boltzmann constant, T is the temperature of the filament, and $\overline{m}$ is the average particle mass. Furthermore, the nonrelativistic MHD momentum equation is:

$$\rho\frac{\mathrm{d}\boldsymbol{u}}{\mathrm{d}t} = \frac{(\boldsymbol{B}\cdot\nabla)\boldsymbol{B}}{\mu_0} - \nabla\left(P + \frac{B^2}{2\mu_0}\right) + \boldsymbol{F}_d, \tag{12}$$

where $\boldsymbol{F}_\mathrm{d}$ is the drag force per unit volume exerted on the filament during motion. In the y-direction, the total pressure of the filament balances the total pressure of the surrounding medium (denoted by the subscript "med"), giving

$$P_\mathrm{med} + \frac{B_\mathrm{med}^2}{2\mu_0} = p + \frac{B^2}{2\mu_0}, \tag{13}$$

where P_med and B_med are obtained directly from the background medium and where P is the thermal pressure of the flux tube under investigation. Assuming that the surrounding medium is in equilibrium, Eq. (12) can be written as:

$$\frac{(\boldsymbol{B}_\mathrm{med}\cdot\nabla)\boldsymbol{B}_\mathrm{med}}{\mu_0} - \nabla\left(P_\mathrm{med} + \frac{B_\mathrm{med}^2}{2\mu_0}\right) = 0. \tag{14}$$

Defining $\Delta\boldsymbol{B} = \boldsymbol{B} - \boldsymbol{B}_\mathrm{med}$ and substituting Eqs. (13) and (14) into Eq. (12) gives

$$\rho\frac{\mathrm{d}\boldsymbol{u}}{\mathrm{d}t} = \frac{(\boldsymbol{B}\cdot\nabla)\Delta\boldsymbol{B}}{\mu_0} + \frac{(\Delta\boldsymbol{B}\cdot\nabla)\boldsymbol{B}_\mathrm{med}}{\mu_0} + \boldsymbol{F}_d. \tag{15}$$

Using Eq. (9), Eq. (15) can be expressed in Lagrangian form as

$$\frac{\partial\boldsymbol{u}(m,t)}{\partial t} = \frac{\Phi}{\mu_0}\frac{\partial\Delta\boldsymbol{B}(m,t)}{\partial m} + \left[\frac{(\Delta\boldsymbol{B}(m,t)\cdot\nabla)\boldsymbol{B}_\mathrm{med}(\boldsymbol{x},t)}{\mu_0\rho(m,t)}\right]_{\boldsymbol{x}=\boldsymbol{x}(m,t)} + \frac{\boldsymbol{F}_d}{\rho}. \tag{16}$$

2.3 Drag estimation

When the filament slides on the xz plane, the background medium resists motion with a small viscous drag. Assuming that the viscous drag is proportional to the velocity of the filament:

$$\boldsymbol{F}_d = -\frac{2\eta\boldsymbol{u}}{f_y R}\frac{\mathrm{d}S}{\mathrm{d}V}, \tag{17}$$

where η is the effective viscosity coefficient, $\mathrm{d}S$ is the cross-sectional area of the filament, R is half the width of the filament in the y-direction, and f_y describes the degree of velocity shear ($0 < f_y < 1$). The effective viscosity coefficient η is approximately

$$\eta = \frac{1}{6}\left[\left(\rho\overline{u}\overline{\lambda}\right) + \left(\rho\overline{u}\overline{\lambda}\right)_\mathrm{med}\right], \tag{18}$$

where $\overline{u}$ is the average thermal velocity and $\overline{\lambda}$ is the mean free path. The parameters on the right-hand side of Eq. (18) are known except for $\overline{\lambda}$ (in a collisionless plasma). In the direction perpendicular to the magnetic field, the mean free path of the plasma does not exceed twice the gyroradius a_c, so we obtain

$$\overline{\lambda} = 2a_c f_c, \tag{19}$$

where f_c is a parameter describing wave–particle interactions ($0 < f_c < 1$). The drag $\boldsymbol{F}_\mathrm{d}$ can be written as

$$\boldsymbol{F}_d = -\frac{2\boldsymbol{u}F_c}{3R_E^2}\left[(\rho u_{th}\overline{a_c}) + (\rho u_{th}\overline{a_c})_\mathrm{med}\right], \tag{20}$$

where

$$F_c = \frac{f_c}{f_y}\left(\frac{R_E^2}{R}\frac{\mathrm{d}S}{\mathrm{d}V}\right), \tag{21}$$

R is the scale of the filament on the equatorial plane perpendicular to magnetic field $\boldsymbol{B}$. In Eq. (20), the parameter F_c includes unknown physical parameters of the filament, as well as wave–particle interactions and turbulence effects.

2.4 Energy equation

One part of the energy entering the filament comes from heat generated by friction at the boundary between the filament and the background medium, and the other part comes from work done by volume changes of the filament. According to energy conservation, the first law of thermodynamics for the unit mass of the filament is

$$\frac{3}{2}\frac{k}{\overline{m}}\frac{\partial T(m,t)}{\partial t} = -P\frac{\partial}{\partial t}\left(\frac{1}{\rho}\right) + \frac{f_h F_d u}{\rho}, \tag{22}$$

where f_h is the proportion of frictional heat entering the filament ($0 < f_h < 1$). The three vectors $\boldsymbol{x}(m,t)$, $\boldsymbol{u}(m,t)$, and $\boldsymbol{B}(m,t)$ and the three scalars P, T, and ρ can be determined via vector equations (7), (10), and (16) and scalar equations (11), (13), and (22).

2.5 Boundary conditions

A finite conductor is placed at the Earth boundary in our calculations as an approximation of the conducting ionosphere. There is a current on each side of the filament:

$$\boldsymbol{J}_\mathrm{side} = \mu_0^{-1}\Delta\boldsymbol{B}\times\hat{\boldsymbol{n}}, \tag{23}$$

where $\hat{\boldsymbol{n}}$ is the outward normal. The interaction between the Earth's magnetic field and solar wind generates Pedersen currents. $\boldsymbol{J}_\mathrm{side}$ and the Pedersen current $\Sigma_p\boldsymbol{E}_b$ form a complete circuit. A boundary condition on the Earth-side plane can be derived from the relationship between the boundary electric field and the z-component of the filament velocity at the boundary:

$$E_y = \frac{\delta B_z}{\mu_0\Sigma_p} = \dot{z}B_x, \tag{24}$$

where Σ_p is the conductivity, which is set to 4 mhos; B_x and B_z denote the magnetic field components in the x-direction and z-direction, respectively; the x-component of the filament velocity v_x is assumed to be zero. Owing to symmetry, it is assumed that B_x and the z-component of the velocity v_z are both zero when the filament crosses the equatorial plane.

3 Numerical simulation

3.1 Numerical methods

The Lagrangian method is employed in our investigation. The

CSTR: 32290.14.JUSTC-2025-0077
DOI: 10.52396/JUSTC-2025-0077
JUSTC, **2025**, 55(X):

filament is treated as a line composed of 250 elements. Numerical simulation is used to obtain the time evolution of the physical parameters for each element and thus the time evolution of the entire filament. From the filament motion equations in Section 2, given the position $\boldsymbol{x}_i$, velocity $\boldsymbol{u}_i$, pressure P_i, temperature T_i, density ρ_i, magnetic field $\boldsymbol{B}_i$ and parameters including the drag of the ith particle element at time t, we can calculate $\boldsymbol{x}_i$, $\boldsymbol{u}_i$, and T_i of the "i"th particle element at time $t+\triangle t$ through Eqs. (7), (12), and (22). These are then substituted into Eqs. (10), (11), and (13) to obtain the pressure P_i, magnetic field $\boldsymbol{B}_i$ and, density ρ_i at time $t+\triangle t$, completing the update of all the parameters. Central difference schemes are used to represent the spatial derivative.

3.2 Parameter settings

The temperature of the background medium is set to 5 keV, and the height of the ionosphere is set to 5 $R_{\rm E}$. From the THEMIS spacecraft, Refs. [23, 24] reported that the ion and electron temperatures increase by 6–10 times and that the specific entropies increase by 20 times when the magnetopause from the magnetosheath to the plasma sheet is crossed. The specific entropy is defined as

$$s = P/N^{5/3}, \tag{25}$$

where N is the plasma number density. On the basis of these observational data, the temperature inside the part of the flux tube with magnetosheath content is set to 800 eV, and the number density is set to 2.5 times that of the magnetosphere. The friction coefficient f_c is set to 0.6, and the heat conversion coefficient f_h is set to 0.

The 50 points near the equator are set with magnetosheath parameters, and the remaining 200 points are set with magnetospheric parameters.

3.3 Results and analysis

As a reference, Fig. 1 shows the background magnetic field lines in the plasma sheet. The magnetic field and pressure are derived from the background model in Section 2.1. This background medium is in the equilibrium state.

Fig. 2 shows magnetic flux tubes with initial positions at 25 $R_{\rm E}$, 35 $R_{\rm E}$, 45 $R_{\rm E}$ and 55 $R_{\rm E}$ and their final equilibrium positions. Two points can be clearly observed. One is their closer final locations to the Earth, and the other is their dipolar shape, which is greater than their initial shape. Under prolonged northward IMF, vortex structures that developed in the nonlinear stage of KHI at the Earth's magnetopause would induce conjugate reconnection. The part of the magnetospheric flux tube near the equator is replaced with a part of the magnetosheath flux tube, resulting in a low-entropy magnetic flux tube in the Earth's LLBL. Observations clearly revealed that the magnetic field in the flank decreases as the spacecraft travels from the magnetosheath to the magnetosphere[25]. When a small part of the magnetospheric flux tube is replaced by a part of the magnetosheath flux tube, the cross-sectional area of the original magnetosperic flux tube is replaced with a smaller magnetosheath area. The volume V along the flux tube decreases. Thus, the total entropy $PV^{5/3}$ of the newly formed flux tube is lower than that of the surrounding tube, forming a low-entropy flux tube. This leads to interchange instability. The motion of magnetic flux tubes under interchange instability can be described by magnetic filament theory[26, 27]. In this theory, the motion of a magnetic filament primarily depends on its $PV^{5/3}$ value. If the $PV^{5/3}$ of the newly formed flux tube is greater than that of the surrounding medium, it will move toward the Earth's magnetotail; if it is smaller, it will move toward the Earth. The flux tube continues moving until it reaches an equilibrium position in the plasma sheet where its $PV^{5/3}$ equals that of adjacent flux tubes.

Fig. 3 shows the time series of the position and shape of a low-entropy magnetic flux tube with its initial position at 40

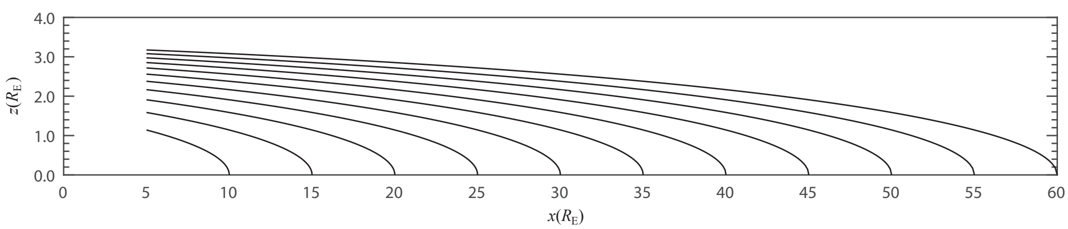

Fig. 1. Magnetic field lines of the background equilibrium medium. The temperature is set uniformly at 5 keV. The Earth is on the left side of the boundary. Only half of the plasma sheet is presented. Symmetry about the equator is assumed.

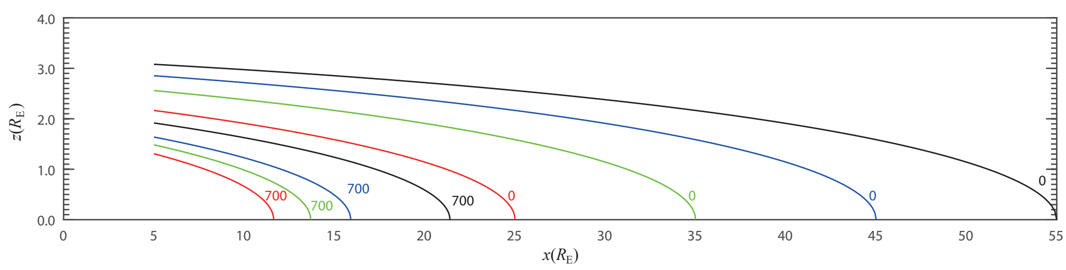

Fig. 2. Magnetic flux tubes with their initial positions at 25 $R_{\rm E}$, 35 $R_{\rm E}$, 45 $R_{\rm E}$, and 55 $R_{\rm E}$ and the final equilibrium positions. The magnetic field line labeled '0' is the initial position of the flux tube, and that labeled '700' is its final position. The same color represents the same flux tube. All the final positions of the flux tubes are closer to the Earth than their initial positions are. The final shapes of the field lines are more dipolar than their initial shapes are, inferring a more dipolar and shrinking configuration of the magnetosphere some time later.

CSTR: 32290.14.JUSTC-2025-0077
DOI: 10.52396/JUSTC-2025-0077
JUSTC, **2025**, 55(X):

R_E. The near-equatorial part of the flux tube first accelerates toward the Earth and then decelerates. During motion, the magnetic filament continuously contracts inward, intensifying magnetic field dipolarization. Fig. 4 shows the time evolution of the plasma pressure in the filament. The initial pressure of the filament is lower than that of the background medium. As the filament moves, its pressure gradually approaches and finally equals the background pressure, at which point the filament stops moving. The filament moves toward the Earth because its initial thermal pressure is lower than that of the surrounding flux tubes. For total pressure balance, the magnetic field of the filament is greater than that of the background medium. The magnetic tension of the filament, which is greater than that of the background medium, pulls it toward the Earth. This indicates that under the northward IMF, particles of the magnetosheath enter the magnetotail via conjugate reconnection in the nonlinear stage of KHI at the magnetopause flanks, forming low-entropy magnetic flux tubes. These low-entropy flux tubes begin to move toward the Earth. This finding is consistent with the results of Sorathia et al.[19] who used test particle simulations to study the time evolution of low-entropy bubbles.

The earthward motion of magnetic flux tubes at the magnetospheric flanks under the northward IMF has some observational support. Fig. 5 shows a cartoon of the convection pattern in the northern polar cap derived from the observa-

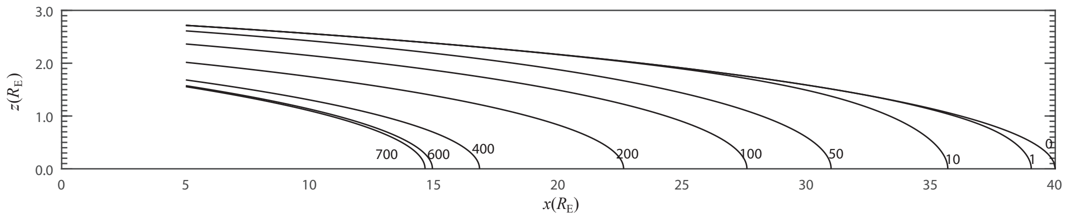

Fig. 3. Positions of the magnetic flux tube at 1, 10, 50, 100, 200, 400, 600, and 700 minutes. The magnetic field line labeled ‘0’ is its initial position at $40R_E$. It stops at 700 min at a position 14.6 R_E from the Earth, a location that is closer to the Earth than its initial location. The final shape of the flux tube is more dipolar than its initial shape.

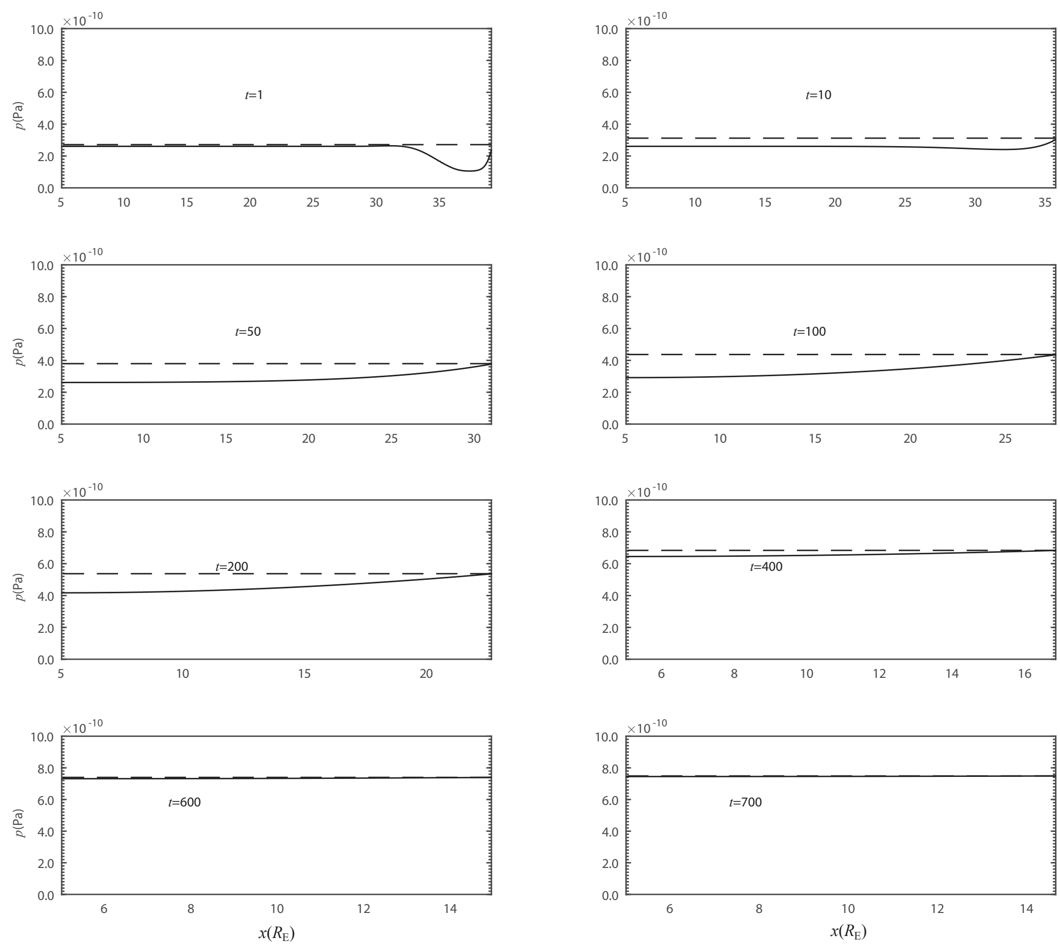

Fig. 4. The time series of plasma pressure along the filament with its initial position at 40 R_E. The solid line represents the pressure in the filament, and the dashed line represents the background pressure. Initially, the pressure in the filament is lower than that of the background. Owing to its motion toward the Earth, the pressure in the flux tube increases and finally reaches the background value.

CSTR: 32290.14.JUSTC-2025-0077
DOI: 10.52396/JUSTC-2025-0077
JUSTC, **2025**, 55(X):

tional dawn–dusk electric field distribution under the northward IMF[28]. The convection pattern in one ionospheric hemisphere is simplified into four convective cells. The plasma flows sunward in the central polar cap and antisunward in the polar cap flanks. Fig. 6 shows the Earth's magnetic field lines of the International Geomagnetic Reference Field (IGRF) model. Under the northward IMF, the Earth's magnetosphere is composed of closed magnetic field lines. The outermost layer of the magnetic field lines corresponds to the magnetopause, which maps its foot to the central polar cap. From the sunward convection in the central polar cap, we can infer a corresponding sunward flow in the LLBL, which is consistent with our simulation results.

Fig. 7 shows the density of the filament at 10, 50, 100, 200, 400, 600, and 700 min with an initial position at $40R_E$. As the filament moves toward the Earth, its density gradually increases, which is consistent with the particle distribution in the *xz*-plane obtained by Zhao[29] via test particle simulations under the northward IMF. It can be inferred that the increased density results from magnetosheath particles entering the Earth's plasma sheet via reconnection at the flanks. The cliff drop in particle density along each line marks the boundary between the magnetospheric and magnetosheath particles.

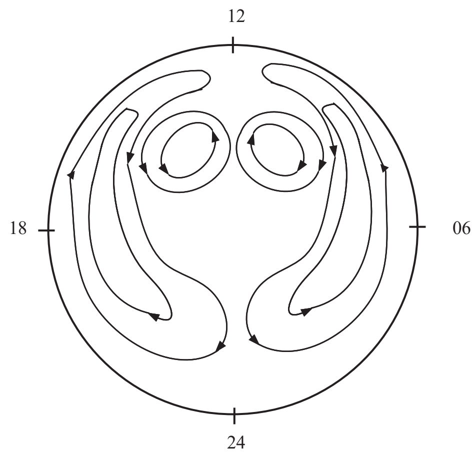

Fig. 5. Cartoon of the convection pattern in the northern polar cap inferred from the measured electric field under northward IMF conditions. Four convection cells are suggested.

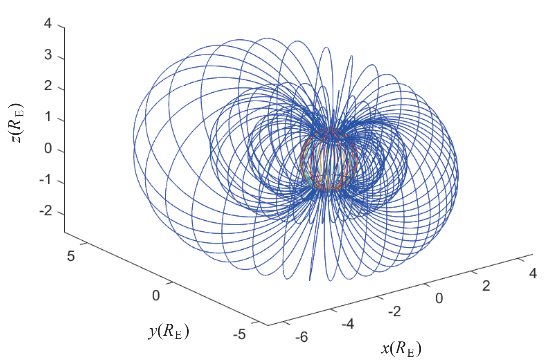

Fig. 6. Diagram of the Earth's magnetic field lines derived from the international geomagnetic reference field model. The outermost layer represents the magnetopause, with its field line feet rooted in the center of the polar cap.

Typically, the density of magnetosheath particles is greater than that of magnetospheric particles. Under northward IMF, a typical feature is the formation of a dense plasma sheet. Although our simulations are on some magnetic field lines, the accumulation of such field lines with different initial positions contributes to the formation of a dense plasma sheet. A basic feature of CDPS events is a particle density greater than 1 cm^{-3}. The simulation results reveal that the stationary density of magnetosheath particles in the magnetosphere is greater than 1 cm^{-3}.

Fig. 8 shows the temperature of the filament at 10, 50, 100, 200, 400, 600, and 700 min with the same initial position. The temperature of the magnetosheath part of the filament is always lower than the background temperature (5 keV). Particles entering the plasma sheet from the flanks are cold. The KHI provides a mechanism for filling a plasma sheet

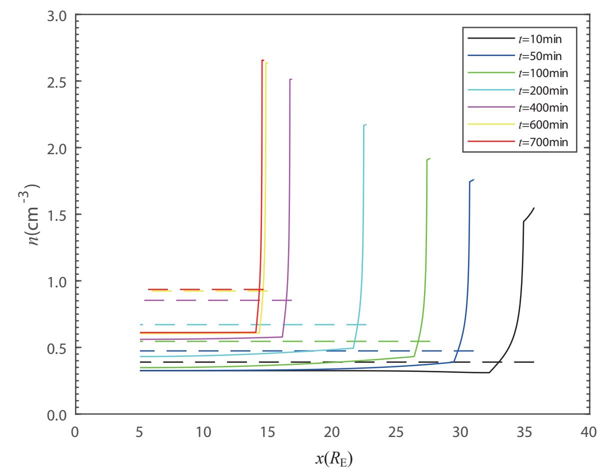

Fig. 7. Time series of the plasma density along the filament with its initial position at 40 R_E. The solid lines represent the density in the filament, and the dashed lines represent the background density. The density increases as the filament moves toward the Earth. The density near the equator is much greater than that of the background.

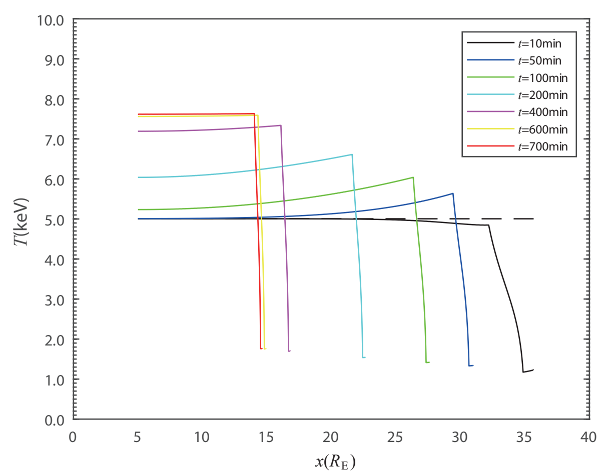

Fig. 8. Time series of the plasma temperature along the filament with its initial position at 40 R_E. The solid lines represent the temperature in the filament, and the black dashed line represents the background temperature. Although the temperature increases as the filament moves toward the Earth, the temperature near the equator is much lower than that of the background.

CSTR: 32290.14.JUSTC-2025-0077
DOI: 10.52396/JUSTC-2025-0077
JUSTC, **2025**, 55(X):

with cold plasma.

Some waves appear in Figs. 3 and 4. These waves are MHD waves. In particular, they are Alfven waves perpendicular to the filament and slow mode waves along it. Since a pressure balance between the filament and background medium is imposed, the fast mode wave does not appear.

Satellite observations have shown that during northward IMF, plasma in the Earth's plasma sheet becomes cold and dense, which is attributed to the massive transport of solar wind or magnetosheath ions into the plasma sheet[30]. Our simulation covers an initial range of 25 R_E ~ 50 R_E, which is consistent with the suggestion of Terasawa et al.[31] that the increase in magnetotail particle density under northward IMF occurs in the region 15 $R_E < x < 50$ R_E.

4 Conclusions

To further demonstrate that KHI in the LLBL is the main pathway for solar wind plasma to enter the Earth's magnetosphere under the northward IMF, this study simulates the motion of magnetic flux tubes in the magnetospheric flanks. These flux tubes are generated by conjugate reconnection in the nonlinear stage of KHI at the magnetospheric flanks. The flux tubes in this study are produced by replacing part of the magnetospheric flux tube near the equator with part of the magnetosheath flux tube. Through MHD numerical simulations, we obtained the time-dependent characteristics of the flux tubes. Owing to the initial total entropy of the magnetic flux tube being lower than that of the adjacent magnetospheric flux tube, it moves toward the Earth until its internal pressure equals that of the surrounding background medium. The sunward motion of these conjugate reconnection-generated flux tubes along the magnetospheric flanks is consistent with the typical four-cell convection pattern in the polar cap under northward IMF, where the flow in the central polar cap is sunward. Analysis of the simulation results also reveals that the transfer of magnetosheath particles into the Earth's magnetosphere contributes to the formation of a typical cold and dense plasma sheet under the northward IMF. This research provides theoretical support for an in-depth understanding of the interaction between solar wind and the Earth's magnetosphere under northward IMF conditions.

Our numerical simulations do not involve magnetic reconnection, and heating from magnetic reconnection is not included in the calculation equations. In the 1D filament, only momentum is transferred between adjacent nodes, with no mass or heat exchange, resulting in a distinct interface between the magnetosheath-originated part and the magnetosphere-originated part. The injection of magnetosheath particles into the magnetosphere is gradual, with each conjugate reconnection adding a small amount. Over time, with convection taking part in, a cold and dense plasma sheet finally forms. In total, we discuss the motion law of magnetic flux tubes produced by KHI mechanism and how these magnetic flux tubes contribute to the formation of a cold and dense plasma sheet. In the future, we try to build a 3D background model. In this model, we can investigate the influence of KHI on dawn–dusk temperature and density asymmetries through the motion of 1D magnetic flux tube. We can further combine the satellite observation data to study how KH growth rate and reconnection efficiency affect particle transport.

Acknowledgements

This work was supported by the National Natural Science Foundation of China (NSFC41974204).

Conflict of interest

The authors declare that they have no conflict of interest.

Biographies

Xinling Ma is a graduate student for master degree at the School of Earth and Space Sciences, University of Science and Technology of China. Her research mainly focuses on magnetosheric physics.

Chuxin Chen is a Professor at the School of Earth and Space Sciences, University of Science and Technology of China. He received his Ph.D. degree in Space Physics and Astronomy from Rice University in 1995. His research mainly focuses on magnetospheric physics and planetary physics.

References

[1] Dungey J W. Interplanetary magnetic field and the auroral zones. *Physical Review Letters*, **1961**, *6* (2): 47–48.
[2] Romain M, Nicolas A, Hiroshi H, et al. Magnetospheres in the Solar System. Hoboken, NJ, USA: Wiley, **2021**.
[3] Faganello M, Califano F, Pegoraro F, et al. Magnetic reconnection and Kelvin–Helmholtz instabilities at the Earth's magnetopause. *Plasma Physics and Controlled Fusion*, **2012**, *54* (12): 124037.
[4] Lu J Y, Jing H, Liu Z Q, et al. Energy transfer across the magnetopause for northward and southward interplanetary magnetic fields. *Journal of Geophysical Research: Space Physics*, **2013**, *118* (5): 2021–2033.
[5] Zhang H X, Lu J Y, Wang M. Energy transfer across magnetopause under dawn–dusk IMFs. *Scientific Reports*, **2023**, *13* (1): 7409.
[6] Guo J L, Shen C, Liu Z X. Simulation of magnetc reconnection on the magnetopause under northward IMF condition. *Progress in Geophysics*, **2013**, *28* (2): 540–544. (in Chinese)
[7] Hasegawa H, Fujimoto M, Phan D T, et al. Transport of solar wind into Earth's magnetosphere through rolled-up Kelvin–Helmholtz vortices. *Nature*, **2004**, *430* (7001): 755–758.
[8] Lin Y, Johnson J R, Wang X. Three-dimensional mode conversion associated with Kinetic Alfvén waves. *Physical Review Letters*, **2012**, *109* (12): 125003–125003.
[9] Lemaire J, Roth M. Penetration of solar wind plasma elements into the magnetosphere. *Journal of Atmospheric and Terrestrial Physics*, **1978**, *40* (3): 331–335.
[10] Wing S, Johnson J R, Chaston C C, et al. Review of solar wind entry into and transport within the plasma sheet. *Space Science Reviews*, **2014**, *184* (1–4): 33–86.
[11] Stenuit H, Fujimoto M, Fuselier A S, et al. Multispacecraft study on the dynamics of the dusk–flank magnetosphere under northward IMF: 10–11 January 1997. *Journal of Geophysical Research: Space Physics*, **2002**, *107* (A10): SMP 27-1–SMP 27-14.
[12] Kavosi S, Raeder J. Ubiquity of Kelvin–Helmholtz waves at Earth's magnetopause. *Nature Communications*, **2015**, *6*: 7019.
[13] Chen C X. Preservation and variation of ion-to-electron temperature ratio in the plasma sheet in geo-magnetotail. *Earth and Planetary Physics*, **2021**, *5* (4): 337–347.
[14] Nykyri K, Otto A. Plasma transport at the magnetospheric boundary

due to reconnection in Kelvin–Helmholtz vortices. *Geophysical Research Letters*, **2021**, *28* (18): 3565–3568.
[15] Li W, André, M, Khotyaintsev Y V, et al. Kinetic evidence of magnetic reconnection due to Kelvin–Helmholtz waves. *Geophysical Research Letters*, **2016**, *43* (11): 5635–5643.
[16] Johnson J R, Wing S. Northward interplanetary magnetic field plasma sheet entropies. *Journal of Geophysical Research: Space Physics*, **2009**, *114* (A9): A00D08.
[17] Nykyri K, Otto A, Lavraud B, et al. Cluster observations of reconnection due to the Kelvin–Helmholtz instability at the dawnside magnetospheric flank. *Annales Geophysicae*, **2006**, *24* (177): 2619–2643.
[18] Guo X C , Wang C , Hu Y Q. Global MHD simulation of the Kelvin–Helmholtz instability at the magnetopause for northward interplanetary magnetic field. *Journal of Geophysical Research Space Physics*, **2010**, *115*: A10218.
[19] Sorathia K A, Merkin V G, Ukhorskiy A Y, et al. Solar wind ion entry into the magnetosphere during northward IMF. *Journal of Geophysical Research: Space Physics*, **2019**, *124*(7): 5461–5481.
[20] Pontius D H, Wolf R A. Transient flux tubes in the terrestrial magnetosphere. *Geophysical Research Letters*, **1990**, *17* (1): 49–52.
[21] Voigt G H. Magnetospheric equilibrium configurations and slow adiabatic convection. *Solar Wind Magnetosphere Coupling*, **1986**, *126*: 233.
[22] Fuchs K, Voigt G H. Self-consistent theory of a magnetospheric B-field model. In: Quantitative Modeling of Magnetospheric Processes. Washington D C: American Geophysical Union (AGU), **1979**, 21: 86–95.
[23] Wang C, Gkioulidou M, Lyons R L, et al. Spatial distributions of the ion to electron temperature ratio in the magnetosheath and plasma sheet. *Journal of Geophysical Research: Space Physics*, **2012**, *117*: A08215.
[24] Wing S, Newell P T. 2D plasma sheet ion density and temperature profiles for northward and southward IMF. *Geophysical Research Letters*, **2002**, *29* (16): 21-1–21-4.
[25] Taylor M G G T, Lavraud B. Observation of three distinct ion populations at the Kelvin-Helmholtz-unstable magnetopause. *Annales Geophysicae*, **2008**, *26* (6): 1559–1566.
[26] Chen C X, Wolf R A. Interpretation of high-speed flows in the plasma sheet. *Journal of Geophysical Research Space Physics*, **1993**, *98* (A12): 21409–21419.
[27] Chen C X, Wolf R A. Theory of thin-filament motion in Earth's magnetotail and its application to bursty bulk flows. *Journal of Geophysical Research*, **1999**, *104*: 14613–14626.
[28] Burke W J, Kelley M. C, Sagalyn R C, et al. Polar cap electric field structures with a northward interplanetary magnetic field. *Geophysical Research Letters*, **1979**, *6* (1): 21–24.
[29] Zhao M X. Particle Simulation of solar wind transport into the magnetosphere during northward IMF. *Chinese Journal of Space Science*, **2022**, *42* (6): 1068–1078. (in Chinese)
[30] Øieroset M , Raeder J , Phan D T, et al. Global cooling and densification of the plasma sheet during an extended period of purely northward IMF on October 22–24, 2003. *Geophysical Research Letters*, **2005**, *32* (12): L12S07.
[31] Terasawa T, Fujimoto M, Mukai T, et al. Solar wind control of density and temperature in the near-Earth plasma sheet: WIND/GEOTAIL collaboration. *Geophysical Research Letters*, **1997**, *24* (8): 935–938.

CSTR: 32290.14.JUSTC-2025-0077
DOI: 10.52396/JUSTC-2025-0077
JUSTC, **2025**, 55(X):